ETH
Eidgenössische Technische Hochschule Zürich
Swiss Federal Institute of Technology Zurich

Seminar for Applied Mathematics SAM

A well-balanced scheme for the Euler equations with gravitation

R. Käppeli

Research Report No. 2016-53
December 2016

Seminar für Angewandte Mathematik
Eidgenössische Technische Hochschule
CH-8092 Zürich
Switzerland

A well-balanced scheme for the Euler equations with gravitation

Roger Käppeli

Abstract We present a novel well-balanced scheme for the Euler equations with gravitation. The scheme is designed to preserve exactly an isothermal hydrostatic equilibrium. It uses a novel equilibrium preserving reconstruction based on the Gibbs free energy. Moreover, the developed scheme is applicable beyond the ideal gas law which is crucial for many astrophysical applications. The scheme is second-order accurate in space and can easily be implemented into any existing code solving time explicitly or implicitly the Euler equations. We assess the performance of the scheme on two test problems involving a realistic equation of state for stellar matter.

1 Introduction

Many interesting astrophysical phenomena can be modeled by the Euler equations with gravitational source terms

$$\frac{\partial \rho}{\partial t} + \nabla \cdot (\rho \mathbf{v}) = 0 \tag{1}$$

$$\frac{\partial \rho \mathbf{v}}{\partial t} + \nabla \cdot (\mathbf{v} \rho \mathbf{v}) + \nabla p = -\rho \nabla \phi \tag{2}$$

$$\frac{\partial E}{\partial t} + \nabla \cdot [(E + p)\mathbf{v}] = -\rho \mathbf{v} \cdot \nabla \phi \tag{3}$$

expressing the conservation of mass, momentum and energy, respectively. Here ρ is the mass density, $\mathbf{v}$ the velocity and $E = \rho e + \rho v^2/2$ the total (fluid) energy density being the sum of internal and kinetic energy density. The system is closed by an

Roger Käppeli
ETH Zürich, Seminar for Applied Mathematics, Rämistrasse 101, CH-8092 Zürich,
e-mail: roger.kaeppeli@sam.math.ethz.ch

equation of state (EoS) relating the pressure $p = p(\rho, e)$ to the density and specific internal energy.

The source terms on the right hand side of the momentum and energy equations model the effect of gravity forces onto the fluid. They are given in terms of the gradient of the gravitational potential ϕ which may either be a given function or, in case of self-gravity, is the solution of the Poisson equation

$$\nabla^2 \phi = 4\pi G \rho, \tag{4}$$

where G is the gravitational constant.

Numerical methods for the Euler equations are in a major stage of development for a vast range of flow regimes. Among the most popular schemes are the so-called Godunov-type finite volume methods. We refer to e.g. [14, 16, 24] for a comprehensive introduction. In these schemes, the cell averages of the conserved variables are evolved in terms of numerical fluxes. The latter are determined by approximate or exact solutions of Riemann problems at each cell interface. High order spatial accuracy is provided by suitable non-oscillatory polynomial reconstruction procedures such as TVD, ENO and WENO reconstructions (see e.g. [21]). High order temporal accuracy is achieved by appropriate ODE integrators such as the strong stability preserving (SSP) Runge-Kutta schemes (see e.g. [9]).

In astrophysics it often happens that the flow of interest is close to hydrostatic equilibrium

$$\nabla p = -\rho \nabla \phi. \tag{5}$$

Such conditions arise for example in the simulation of waves in the atmosphere of our sun, convective nuclear burning during stellar evolution and in the dramatic death of a star in a supernova. The numerical approximation of near equilibrium flows turns out to be challenging for standard numerical methods. The reason behind these difficulties is the fact that they do not necessarily satisfy a discrete version of the balance between the pressure gradient and gravity forces. Consequently, equilibrium states are not preserved exactly but are approximated with an error proportional to the truncation error. So if one is interested in simulating small perturbations of the equilibrium, the numerical resolution has to be increased to the point that truncation errors do not obscure the phenomena of interest. Especially in multiple dimensions, the required resolution may become prohibitively large.

In order to overcome this challenge, Greenberg and Leroux [10] introduced the concept of well-balanced schemes. In these schemes, a discrete balance is satisfied at steady states. For instance, many well-balanced schemes have been designed for the shallow water equations with bottom topography, see e.g. [1, 15, 20]. A comprehensive review on well-balanced schemes in many applications is also given in the book by Gosse [8].

Well-balanced schemes for hydrostatic equilibrium have received considerable attention in the recent literature [17, 3, 7, 26, 11, 25, 6, 5, 18, 19, 12]. However, it turns out that Eq. (4) only defines a mechanical equilibrium. A further assumption on a thermodynamic equilibrium is needed in order to uniquely specify the hydrostatic equilibrium. Two physically relevant cases are the isentropic and isothermal

equilibria assuming constant entropy or temperature, respectively. In this contribution we focus on the latter one. Such conditions arise for example in the interior of white dwarf stars due to the high thermal conductivity of degenerate electrons (see e.g. [13]). Well-balanced schemes for isothermal hydrostatic equilibrium have presented in [7, 26, 5, 18, 19] assuming an ideal gas EoS. This limits their applicability to more complex astrophysical scenario quite strongly. Therefore we present here an approach that works with any EoS. Our approach closely follows the one by Käppeli & Mishra [11]. Actually, only the thermodynamic potential for the local hydrostatic reconstruction has to be changed. To keep the present contribution compact and because the developments here follow the latter reference very closely, we present below only the strictly necessary modifications of [11].

The rest of the article is organized as follows: the well-balanced scheme is presented in section 2, numerical results are reported in section 3 and we conclude in section 4.

2 Numerical methods

For the sake of simplicity, we present the well-balanced scheme in a one-dimensional setting. Pointers to the literature for multidimensional extension are given at the end of the section.

In one spatial dimension, the Euler equations are given by

$$\frac{\partial \mathbf{u}}{\partial t} + \frac{\partial \mathbf{F}}{\partial x} = \mathbf{S} \tag{6}$$

where

$$\mathbf{u} = \begin{bmatrix} \rho \\ \rho v_x \\ E \end{bmatrix}, \quad \mathbf{F} = \begin{bmatrix} \rho v_x \\ \rho v_x^2 + p \\ (E+p)v_x \end{bmatrix} \quad \text{and} \quad \mathbf{S} = - \begin{bmatrix} 0 \\ \rho \\ \rho v_x \end{bmatrix} \frac{\partial \phi}{\partial x}, \tag{7}$$

are the vectors of conserved variables, fluxes and source terms, respectively. Furthermore, we denote the primitive variables by $\mathbf{w} = [\rho, v_x, p]^T$.

2.1 One-dimensional finite volume method

For the numerical approximation of solutions to Eq. (6), the spatial domain is discretized into finite volumes or cells $I_i = [x_{i-1/2}, x_{i+1/2}]$. For ease of presentation, we take the cells I_i to be of regular sizes $\Delta x = x_{i+1/2} - x_{i-1/2}$ with centers $x_i = (x_{i-1/2} + x_{i+1/2})/2$. The integration of Eq. (6) over a cell I_i then results in a semi-discrete finite volume scheme for the evolution of the cell averaged conserved variables

$$\frac{\mathrm{d}\mathbf{u}_i}{\mathrm{d}t} = \mathbf{L}(\mathbf{u}) = -\frac{1}{\Delta x}\left(\mathbf{F}_{i+1/2} - \mathbf{F}_{i-1/2}\right) + \mathbf{S}_i, \tag{8}$$

where the $\mathbf{F}_{i\pm1/2}$ are the numerical fluxes at cell interfaces and $\mathbf{S}_i$ is the cell averaged gravity source term.

The numerical fluxes are obtained by solving (approximately) Riemann problems at cell interfaces

$$\mathbf{F}_{i+1/2} = \mathscr{F}(\mathbf{w}_{i+1/2-}, \mathbf{w}_{i+1/2+}), \tag{9}$$

where the $\mathbf{w}_{i+1/2-}$ and $\mathbf{w}_{i+1/2+}$ denote the cell interface extrapolated primitive variables. For the hydrostatic well-balanced scheme elaborated below we require standard properties such as that the numerical flux $\mathscr{F}$ is consistent, i.e. $\mathscr{F}(\mathbf{w},\mathbf{w}) = \mathbf{F}(\mathbf{w})$, and Lipschitz continuous. In the numerical example presented below, we use the HLLC Riemann solver with wave speed estimates according to Batten et al. [2].

In traditional schemes (at least the ones most commonly used in astrophysics), the gravitational source term is approximated by standard second-order central differences

$$\mathbf{S}_i = -\begin{bmatrix} 0 \\ \rho_i \\ (\rho v_x)_i \end{bmatrix} \frac{\phi_{i+1} - \phi_{i-1}}{2\Delta x}, \tag{10}$$

where the ϕ_i are the cell centered values of the gravitational potential.

The cell interface extrapolated variables $\mathbf{w}_{i\pm1/2\mp}$ are generally obtained by some reconstruction procedure from the cell averages $\mathbf{u}_i$. Commonly, some non-oscillatory piece-wise polynomial reconstruction, such as TVD, ENO or WENO, is used (see e.g. [24] and references therein). Unfortunately, these reconstructions are not well suited for the case considered here. The reason for this is simply the fact that the steady states of interest are generally not piece-wise polynomial functions. In the following section, we build an equilibrium respecting reconstruction that in conjunction with a special momentum source discretization automatically fulfills a discrete version of certain steady states.

A fully discrete finite volume scheme is obtained by discretizing the temporal domain into suitably sized time steps $\Delta t^n = t^{n+1} - t^n$ where the superscript n labels the different time levels. For the schemes developed below, any adequate explicit or implicit time integrator for the system of ordinary differential equations (8) could be used. However, in the numerical results below we use the explicit second-order strong stability preserving (SSP) Runge-Kutta methods (see e.g. [9]):

$$\begin{aligned} \mathbf{u}_i^{(1)} &= \mathbf{u}_i^n + \Delta t^n \mathbf{L}(\mathbf{u}^n) \\ \mathbf{u}_i^{(2)} &= \mathbf{u}_i^{(1)} + \Delta t^n \mathbf{L}(\mathbf{u}^{(1)}) \\ \mathbf{u}_i^{n+1} &= \tfrac{1}{2}\left(\mathbf{u}_i^n + \mathbf{u}_i^{(2)}\right), \end{aligned} \tag{11}$$

where $\mathbf{L}$ is defined in Eq. (8). The time step Δt^n is determined by a suitable CFL condition.

2.2 Local isothermal hydrostatic equilibrium reconstruction and well-balanced source discretization

In the following we first derive an explicit expression for isothermal hydrostatic equilibrium. We start with the well-known thermodynamic relation

$$\mathrm{d}g = \frac{\mathrm{d}p}{\rho} - s\mathrm{d}T, \tag{12}$$

where g is the specific Gibbs free energy

$$g = e + \frac{p}{\rho} - Ts, \tag{13}$$

T the temperature and s the specific entropy. By assuming isothermal conditions and with the above thermodynamic relation Eq. (12) we can express hydrostatic equilibrium Eq. (5) as

$$\frac{\nabla p}{\rho} = \nabla g = -\nabla \phi \tag{14}$$

which can be trivially integrated to yield

$$g + \phi = const. \tag{15}$$

Eq. (15) can then be used to define a local equilibrium reconstruction within each cell I_i as

$$g_{0,i}(x) = g_i + \phi_i - \phi(x) \tag{16}$$

where g_i is simply the Gibbs free energy evaluated from the cell averaged conserved variables $\mathbf{u}_i$ and ϕ_i is the point value of the gravitational potential at cell center. The gravitational potential $\phi(x)$ may either be known as a given function or has to be obtained by some suitable interpolation.

From the local equilibrium reconstruction of the Gibbs free energy $g_{0,i}(x)$, an equilibrium density $\rho_{0,i}(x)$ and pressure $p_{0,i}(x)$ reconstruction can be obtained through the EoS. This is achieved by noting that $g = g(T,p)$ and solving the following equation

$$g_{0,i}(x) = g(T_i, p_{0,i}(x)). \tag{17}$$

This gives an implicit definition of the equilibrium for any $x \in I_i$.

In the case of an ideal gas EoS, $p = \rho RT$, explicit expressions can be given for the equilibrium pressure

$$p_{0,i}(x) = p_i e^{-\frac{1}{RT_i}(\phi(x)-\phi_i)} \tag{18}$$

and density

$$\rho_{0,i}(x) = \frac{p_i}{RT_i} e^{-\frac{1}{RT_i}(\phi(x)-\phi_i)}. \tag{19}$$

In these expression R is the gas constant and T_i (p_i) is simply the temperature (pressure) evaluated from the cell averaged conserved variables $\mathbf{u}_i$. Here we recover the same expressions as [7, 26, 6, 5].

However, the strength of the here presented approach is that it can be used with any EoS, e.g. tabulated, which is highly relevant for computational astrophysics. In this case, the equilibrium pressure and density distribution have to be obtained by some iterative procedure. In order to get the equilibrium pressure distribution $p_{0,i}(x)$, the equation to solve is the following

$$f(p_{0,i}(x)) = g(p_{0,i}(x), T_i) - g_{0,i}(x) = 0. \tag{20}$$

The latter equation can be solved iteratively with a simple Newton-Raphson method

$$\begin{aligned} p_{0,i}^{(k+1)}(x) &= p_{0,i}^{(k)}(x) - f(p_{0,i}(x))/f'(p_{0,i}(x)) \\ &= p_{0,i}^{(k)}(x) - \frac{g(p_{0,i}^{(k)}(x), T_i) - g_{0,i}(x)}{\rho(T_i, p_{0,i}^{(k)}(x))}. \end{aligned} \tag{21}$$

Note that in the last equation, the density $\rho = \rho(T, p)$ has to be computed given a temperature and a pressure through the EoS. The equilibrium density $\rho_{0,i}(x)$ can then also be found once the equilibrium pressure $p_{0,i}(x)$ is found. In the numerical example below, we will use a tabulated EoS that is widely used in astrophysics.

It remains to specify an adequate source term discretization. For the momentum source term, we follow the approach suggested by [1, 3, 7] and define

$$S_{\rho v,i} = \frac{p_{0,i}(x_{i+1/2}) - p_{0,i}(x_{i-1/2})}{\Delta x} \tag{22}$$

where $p_{0,i}(x_{i\pm 1/2})$ are the equilibrium pressures at cell interfaces. We leave the energy source term discretization as in Eq. (10). It can be shown as in [11] that the above expression is a consistent and spatially second-order accurate approximation of the momentum source term.

It is then straightforward to show that the semi-discrete finite volume scheme, Eq. (8), with the above local equilibrium reconstruction and source term discretization is well-balanced with respect to any isothermal hydrostatic equilibrium (see [11]).

Moreover, the scheme can easily be extended to second-order spatial accuracy, multiple dimensions and curvilinear meshes. We refer to [11, 12] for details.

3 Numerical results

In this section we present a series of numerical experiments to demonstrate the performance of the proposed well-balanced scheme. For comparison, we also show results obtained with a standard (unbalanced) base scheme. Moreover, we only present

results obtained with second-order schemes (first-order schemes have little practical use in computational astrophysics).

For all the computations we use the Helmholtz EoS of Timmes & Swesty [23]. It is an astrophysically meaningful EoS including contributions of (photon) radiation, nuclei, electrons and positrons. The radiation is treated as a black body in local thermodynamic equilibrium and the nuclei are modeled by an ideal gas. The electrons and positrons contributions are obtained from a table with a thermodynamically consistent interpolation procedure. The electrons/positrons may have speeds arbitrarily close to relativistic limits and an arbitrary degree of degeneracy. We use the publicly available version of this EoS [22].

3.1 Isothermal hydrostatic atmosphere

As a first numerical experiment, we consider the very simple setting of a one-dimensional isothermal hydrostatic atmosphere in a constant gravitational field

$$\frac{\mathrm{d}p}{\mathrm{d}x} = -\rho g \tag{23}$$

where g is the constant gravitational acceleration[1]. The gravitational potential is then a simple linear function $\phi(x) = gx$.

The computational domain is set to $D = [0, L]$, where $L = 3 \times 10^8$ cm, and is regularly discretized by N cells. Hence, we have the grid size $\Delta x = L/N$, the cell interfaces $x_{i+1/2} = i\Delta x$ and the cell centers $x_i = (x_{i-1/2} + x_{i+1/2})/2$ for $i = 1, ..., N$. For the resolution, we choose $N = 32, 64, 128, 256, 512, 1024, 2048$.

In the following we consider typical white dwarf like conditions. Due to the high thermal conductivity of stellar matter at these conditions, the isothermal hydrostatic equilibrium is an appropriate model. Therefore, we set the gravitational acceleration to $g = 5 \times 10^8$ cm/s^2. For the density and pressure at the base, i.e. $x = 0$, we choose $\rho_0 = 10^7$ g/cm^3 and $p_0 = 8.53 \times 10^{23}$ erg/cm^3. Moreover, the chemical composition is set to half carbon ^{12}C and half oxygen ^{16}O.

The isothermal hydrostatic atmosphere is then initialized over the whole domain D with Eq. (15). Its density and pressure profile are shown in the left panel of Fig. 1. The resulting atmosphere has then a sound crossing time $\tau_{\text{sound}} \approx 2$ s, i.e. a sound wave traverses the atmosphere from base to top and back in a time τ_{sound}. This reflects a time scale on which the equilibrium reacts on perturbations.

For the boundaries we use a hydrostatic equilibrium extrapolation for the density and pressure. See [11] for details. For the velocity we use a simple piece-wise linear extrapolation. This type of boundaries minimize spurious reflection effects as much as possible.

[1] The gravitational acceleration should not be confused with the Gibbs free energy from Section 2.2

We begin by numerically verifying the well-balancing properties of the scheme. For this purpose, we evolve the isothermal atmosphere with the well-balanced and standard (unbalanced) second-order schemes for two sound crossing times, i.e. the final time of the simulation is $t_f = 2\tau_{\text{sound}}$. At the end of the simulation, we compute the L_1-error, i.e. the L_1-norm of the difference between the initial and final state of the simulation. This reflects how well the discrete equilibrium is preserved by the numerical scheme.

In the right panel of Fig. 1 is shown the relative L_1-error for the pressure. The results for the density are similar and are not displayed. From the figure it is clear that the well-balanced scheme is able to maintain the hydrostatic equilibrium down to machine precision. In contrast, the standard scheme is clearly not able to preserve the stationary state. Indeed the error is proportional to its truncation error and scales with the second power of the mesh width, i.e. in accord with its design accuracy.

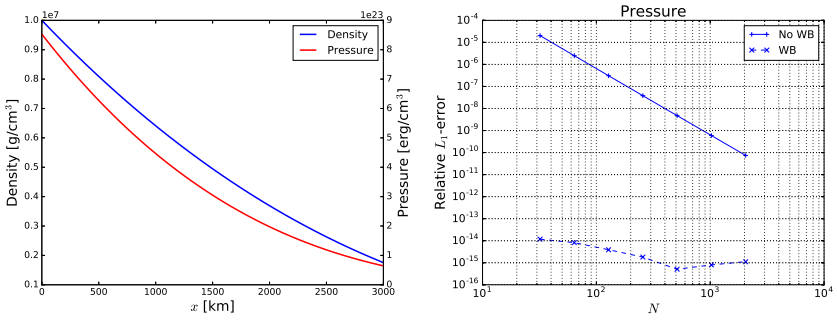

Fig. 1 Left panel: Density and pressure profile of the isothermal hydrostatic atmosphere. Right panel: Relative L_1-norm of the difference between the initial and final state of the simulation. The solid and dashed lines represent the results from the standard and the well-balanced scheme, respectively.

Next we test the ability of the proposed scheme to propagate waves up the atmosphere. For this we impose a periodic velocity perturbation at the base of the atmosphere

$$v_{x,m}^n = A \sin\left(6\frac{2\pi t^n}{t_f}\right), \tag{24}$$

where $m = -1, 0$ is the boundary cell index and A is the wave amplitude.

For the amplitude we choose a small one with $A = 10^3$ cm/s and a large one with $A = 10^7$ cm/s. We then evolve this setting for a time $t_f = 0.45\tau_{\text{sound}}$, i.e. shortly before the waves arrive at the top of the atmosphere.

In Fig. 2 are shown the errors in pressure which have been computed from a reference solution obtained with the well-balanced scheme at resolution $N = 8192$. The errors in density and velocity are similar and not shown. We observe that for the low amplitude case the errors obtained with well-balanced scheme (dashed blue) are much smaller than the ones obtained with the standard scheme (solid blue). For

instance, the well-balanced scheme needs roughly a factor 3-4 less resolution than the standard scheme to reach a given accuracy (for $N \leq 512$). Note that this saving becomes particularly meaningful in a multi-dimensional setting.

The velocity profiles for the small amplitude test are shown in the left panel of Fig. 3. The blue solid line is the reference solution and the solid/dashed red lines are the solutions obtained with the standard and well-balanced schemes at $N = 256$, respectively. From the figure it is clear that the standard scheme suffers some spurious deviations.

For the large amplitude case, the errors in pressure are displayed in Fig. 2 with the red lines. The solid and dashed lines have been computed with the standard and well-balanced schemes, respectively. Here both schemes do equally well and show a first-order convergence. This is expected as the large amplitude waves steepen into shock waves as they propagate up the atmosphere. This is displayed for the velocity in the right panel of Fig. 3. Therefore we note that the well-balanced scheme does not suffer any deterioration in robustness.

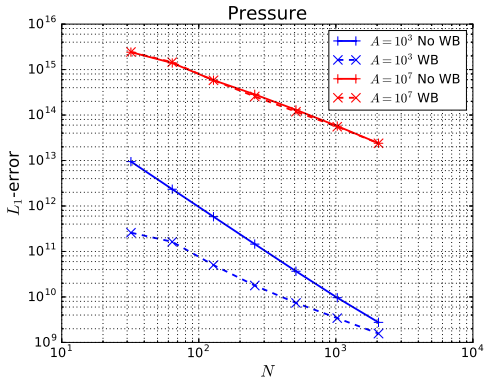

Fig. 2 L_1-norm error in pressure for small (blue lines) and large (red lines) amplitude A perturbations. The reference solutions were computed with the well-balanced scheme and a resolution $N = 8192$. The solid and dashed lines have been obtained with the standard and well-balanced scheme, respectively. Note that here the absolute and not the relative error is shown.

3.2 Rayleigh-Taylor instability

In this example, we simulate the development of a Rayleigh-Taylor instability [4]. We consider the two-dimensional Euler equations Eqs. (1-3) in polar coordinates. Hence, this test demonstrates the ability of the presented scheme to generalize to multiple dimensions and curvilinear coordinates.

The computational domain is $D = [r_{in}, r_{out}] \times [0, 2\pi]$, where $r_{in} = 10^8$ cm and $r_{out} = 4 \times 10^8$ cm. The gravitational potential is purely radial and linear $\phi = \phi(r) = gr$ with $g = 1 \times 10^8$ cm/s^2. At the base, we set the density $\rho_0 = 10^5$ g/cm^3 and the temperature $T_0 = 10^8$ K. At $r_i = 2.5 \times 10^8$ cm we introduce a temperature jump by setting the temperature to $T_1 = 5 \times 10^7$ K for $r \geq r_i$. Again, we set the chemical

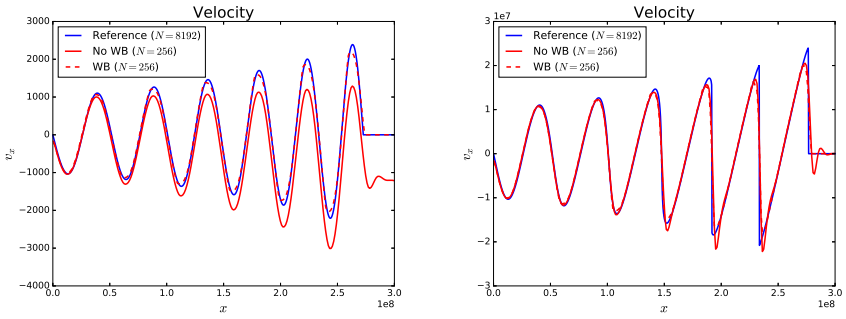

Fig. 3 Velocity profile for the small (left) and large (right) amplitude waves propagating up the isothermal atmosphere. The solid/dashed red lines have been obtained with the standard/well-balanced scheme at resolution $N = 256$. The blue solid line is a reference solution obtained with the well-balanced scheme at resolution $N = 8192$.

composition of the gas to half carbon and half oxygen. The complete equilibrium profile is then obtained by integrating the equation of hydrostatic equilibrium. The resulting profile then has a density jump at r_i that is unstable to the Rayleigh-Taylor instability.

To trigger the instability, we set a velocity perturbation around the interface at r_i

$$v_r(r,\varphi) = 10^{-3} c_s \cos(40\varphi) \exp\left[-100\left(\frac{r-r_i}{r_{out}-r_{in}}\right)^2\right], \tag{25}$$

where c_s is the speed of sound at the interface. The azimuthal velocity v_φ is set to zero everywhere.

We discretize the computational domain D uniformly by $N_r = 100$ radial and $N_\varphi = 300$ azimuthal cells and evolve the initial conditions until final time $t_f = 8$ s. Moreover, for this test we use reflecting boundaries in radial direction and periodic boundaries in azimuthal direction.

The results computed with the well-balanced scheme are shown in Fig. 4. The figure shows the density contours where each quadrant depicts a different time. As seen from the figure, the instability develops slowly and is barely visible at times $t \leq 4$ s. At final time t_f, the Rayleigh-Taylor mushrooms are clearly developed.

Although not shown, the standard scheme has some difficulties especially at following the early development of the instability as it suffers from spurious velocity perturbations due to its inability to resolve hydrostatic equilibrium, i.e. the truncation errors overwhelm the very small velocity perturbation, Eq. (25), imposed to trigger the physical instability. Moreover, at later times the standard scheme also presents some parasitic deviations near the upper and lower radial boundaries again due to its inability to maintain the close to hydrostatic state. This again confirms that well-balanced schemes are superior when the dynamics of interest happen on top of an equilibrium.

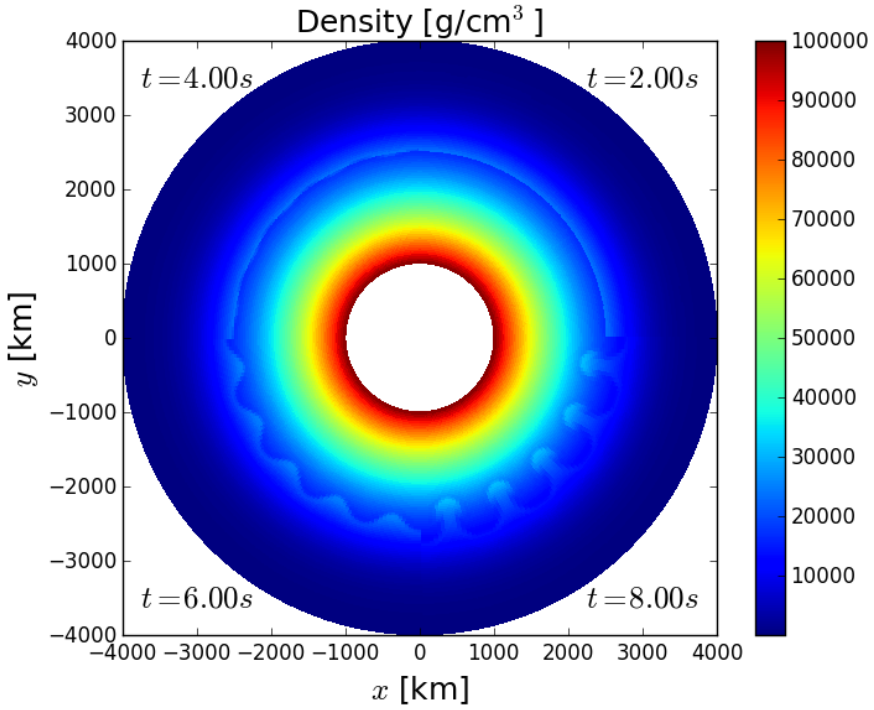

Fig. 4 Density for the Rayleigh-Taylor test problem at different times.

4 Conclusion

We have presented a well-balanced scheme for the Euler equations with gravity. The scheme is able to maintain up to machine precision any isothermal hydrostatic equilibrium. The well-balanced property is achieved by a novel equilibrium preserving reconstruction based on the Gibbs free energy together with a matching momentum sour term discretization. The advantage of the present approach is that it can easily handle complex EoS beyond the ideal gas law. Moreover, it can also be extended to multiple dimensions and curvilinear meshes in a straightforward manner.

The scheme's performance is assessed on astrophysically relevant test cases involving a complex EoS applicable for solar matter in a wide range of conditions. The tests show that the proposed scheme shows some clear advantages over standard unbalanced schemes when the flow of interest is close to an isothermal equilibrium. Away from an equilibrium, the well-balanced scheme recovers the accuracy and robustness of a standard unbalanced scheme.

Acknowledgements We would like to thank Laurent Gosse and Roberto Natalini for organizing the workshop on Innovative Algorithms and Analysis in the enchanting city of Rome. This resulted in many fruitful discussions with researchers from different fields and triggered many new ideas.

References

1. Audusse, E., Bouchut, F., Bristeau, M.O., Klein, R., Perthame, B.: A fast and stable well-balanced scheme with hydrostatic reconstruction for shallow water flows. SIAM Journal on Scientific Computing **25**(6), 2050–2065 (2004).
2. Batten, P., Clarke, N., Lambert, C., Causon, D.M.: On the choice of wavespeeds for the HLLC riemann solver. SIAM Journal on Scientific Computing **18**(6), 1553–1570 (1997).
3. Botta, N., Klein, R., Langenberg, S., Lützenkirchen, S.: Well balanced finite volume methods for nearly hydrostatic flows. Journal of Computational Physics **196**(2), 539 – 565 (2004).
4. Chandrasekhar, S.: Hydrodynamic and Hydromagnetic Stability (International Series of Monographs on Physics (Oxford, England).). Dover Publications (1981)
5. Chandrashekar, P., Klingenberg, C.: A second order well-balanced finite volume scheme for euler equations with gravity. SIAM Journal on Scientific Computing **37**(3), B382–B402 (2015).
6. Desveaux, V., Zenk, M., Berthon, C., Klingenberg, C.: A well-balanced scheme for the Euler equation with a gravitational potential. Springer Proceedings in Mathematics & Statistics p. 217226 (2014).
7. Fuchs, F., McMurry, A., Mishra, S., Risebro, N., Waagan, K.: High order well-balanced finite volume schemes for simulating wave propagation in stratified magnetic atmospheres. Journal of Computational Physics **229**(11), 4033 – 4058 (2010).
8. Gosse, L.: Computing Qualitatively Correct Approximations of Balance Laws. Springer Milan (2013).
9. Gottlieb, S., Shu, C.W., Tadmor, E.: Strong stability-preserving high-order time discretization methods. SIAM Review **43**(1), 89–112 (2001).
10. Greenberg, J., Leroux, A.: A well-balanced scheme for the numerical processing of source terms in hyperbolic equations. SIAM Journal on Numerical Analysis **33**(1), 1–16 (1996).
11. Käppeli, R., Mishra, S.: Well-balanced schemes for the euler equations with gravitation. Journal of Computational Physics **259**(0), 199 – 219 (2014).
12. Käppeli, R., Mishra, S.: A well-balanced finite volume scheme for the Euler equations with gravitation. The exact preservation of hydrostatic equilibrium with arbitrary entropy stratification. Astronomy and Astrophysics **587**, A94 (2016).
13. Kippenhahn, R., Weigert, A., Weiss, A.: Stellar structure and evolution. Astronomy and Astrophysics Library (2012).
14. Laney, C.B.: Computational Gasdynamics. Cambridge University Press (1998)
15. LeVeque, R.J.: Balancing source terms and flux gradients in high-resolution godunov methods: The quasi-steady wave-propagation algorithm. J. Comput. Phys. **146**(1), 346–365 (1998).
16. LeVeque, R.J.: Finite Volume Methods for Hyperbolic Problems (Cambridge Texts in Applied Mathematics), 1 edn. Cambridge University Press (2002).
17. LeVeque, R.J., Bale, D.S.: Wave propagation methods for conservation laws with source terms. In: Hyperbolic problems: theory, numerics, applications, Vol. II (Zürich, 1998), *Internat. Ser. Numer. Math.*, vol. 130, pp. 609–618. Birkhäuser, Basel (1999)
18. Li, G., Xing, Y.: Well-balanced discontinuous galerkin methods for the euler equations under gravitational fields. Journal of Scientific Computing pp. 1–21 (2015).
19. Li, G., Xing, Y.: High order finite volume {WENO} schemes for the euler equations under gravitational fields. Journal of Computational Physics **316**, 145 – 163 (2016).
20. Noelle, S., Pankratz, N., Puppo, G., Natvig, J.R.: Well-balanced finite volume schemes of arbitrary order of accuracy for shallow water flows. J. Comput. Phys. **213**(2), 474–499 (2006).
21. Shu, C.W.: High Order ENO and WENO Schemes for Computational Fluid Dynamics, pp. 439–582. Springer Berlin Heidelberg, Berlin, Heidelberg (1999)
22. Timmes, F.X.: http://cococubed.asu.edu/code_pages/eos.shtml (2013)
23. Timmes, F.X., Swesty, F.D.: The Accuracy, Consistency, and Speed of an Electron-Positron Equation of State Based on Table Interpolation of the Helmholtz Free Energy. Astrophysical Journal Supplement **126**, 501–516 (2000).

24. Toro, E.F.: Riemann Solvers and Numerical Methods for Fluid Dynamics. A Practical Introduction. Springer-Verlag GmbH (1997)
25. Vides, J., Braconnier, B., Audit, E., Berthon, C., Nkonga, B.: A Godunov-type solver for the numerical approximation of gravitational flows. Commun. Comput. Phys. **15**(1), 46–75 (2014)
26. Xing, Y., Shu, C.W.: High order well-balanced WENO scheme for the gas dynamics equations under gravitational fields. J. Sci. Comput. **54**(2-3), 645–662 (2013).